PCCP

Accepted Manuscript

ROYAL SOCIETY OF CHEMISTRY

www.rsc.org/pccp

Journal Name

RSCPublishing

ARTICLE

Heat treatment effect on the electronic and magnetic structures of nanographene sheets investigated through electron spectroscopy and conductance measurements

Cite this: DOI: 10.1039/x0xx00000x

Received 00th January 2012,
Accepted 00th January 2012

DOI: 10.1039/x0xx00000x

www.rsc.org/

Jun-ichi Takashiro, [a] Yasuhiko Kudo, [a] Satoshi Kaneko, [a] Kazuyuki Takai, [a†] Takafumi Ishii, [b] Takashi Kyotani, [b] Toshiaki Enoki, [*a] Manabu Kiguchi [*a]

Heat treatment effect on the electronic and magnetic structures of a disordered network of nanographene sheets has been investigated by *in-situ* measurements of X-ray photoemission spectroscopy, near-edge X-ray absorption fine structure (NEXAFS), and electrical conductance, together with temperature-programmed desorption measurements. Oxygen-containing functional groups bonded to nanographene edges in the pristine sample are almost completely decomposed under heat treatment up to 1300−1500 K, resulting in the formation of edges primarily terminated by hydrogen. The removal of the oxygen-containing groups enhances the conductance owing to the decrease in the electron transport barriers between nanographene sheets. Heat treatment above 1500 K removes also the hydrogen atoms from the edges, promoting the successive fusion of nanographene sheets at the expense of edges. The decrease in the π* peak width in NEXAFS indicates the progress of the fusion reaction, that is, the extension of the π-conjugation, which agrees with the increase in the orbital susceptibility previously reported. The fusion leads to the formation of local π/sp^2 bridges between nanographene sheets and brings about an insulator-to-metal transition at 1500−1600 K, at which the bridge network becomes infinite. As for the magnetism, the intensity of the edge state peak in NEXAFS, which corresponds to the number of the spin-polarized edge states, decreases above 1500 K, though the effective edge-state spin density per edge state starts decreasing approximately 200 K lower than the temperature of the edge state peak change. This disagreement indicates the development of antiferromagnetic short range ordering as a precursor of a spin glass state near the insulator-metal transition, at which the random network of inter-nanographene-sheet exchange interactions strengthened with the formation of the π/sp^2 bridges becomes infinite.

1. Introduction

Nano-sized graphene (nanographene) has attracted increasing interest in both basic and applied sciences in recent years owing to its unconventional electronic structure, which not only provides key issues of fundamental physics and chemistry[1,2] but also enables potential applications such as catalysis, gas sensors, solar cells, and batteries.[2–4] The behavior of electrons on an infinite graphene sheet can be described in terms of massless Dirac fermions moving on a two-dimensional honeycomb bipartite lattice. When a graphene sheet is cut into fragments, the created edges impose boundary conditions on the electrons, and the electronic structure is considerably modified according to the edge geometry, of which the zigzag and armchair geometries are the two extremes. According to theoretical investigations,[2,5] the spin-polarized edge states (non-bonding π states) along the zigzag edge

are created around the Fermi level, with a large local density of states being populated in the vicinity of the edge region, providing nanographene with electronic, chemical, and magnetic activities. In contrast, the armchair edge has no such localized state, and instead electron wave interference takes place, contributing to the stability of nanographene.[2] Consequently, the activities and stability of nanographene depending on the edge geometry enable a variety of functions that lead to potential applications.

The existence of the edge states and their magnetic and electronic properties have been confirmed experimentally for nanographene grown on substrates, graphene nanoribbons, and nanographene-based carbon fibers using various techniques, including scanning tunneling microscopy/spectroscopy (STM/STS), magnetic susceptibility, electron spin resonance (ESR), and near-edge X-ray absorption fine structure (NEXAFS).[6–9] Among existing nanographenes and nanographene-based materials, activated carbon fibers (ACFs) have been particularly important by providing an ideal model for experimental investigations of the edge state and related electronic structures in nanographene.[7,9] ACFs are nanoporous carbon consisting of a three-dimensional disordered network of nanographene sheets with a mean in-plane size of about 3 nm.[10,11] The inter-sheet distance between the nanographene sheets in ACFs (0.38 nm) is considerably larger than that of bulk graphite (0.335 nm), so that the interaction between nanographene sheets is weak in ACFs. Thus, we can study the properties of nanographene using ACFs. The small size of the constituent nanographene sheets leads to a high density of edge carbon atoms in the ACFs. Actually, we have confirmed the existence of the magnetic edge states for ACFs using magnetic susceptibility and NEXAFS measurements, which was facilitated by the sufficiently large amount of edge carbon atoms.[9]

An important issue, which we discuss in the present work, is how nanographene fragments are fused into a larger sheet when they are heat-treated and how this relates to the edge-inherent electronic structure. This is the graphenization process, the opposite of the fragmentation process. What is interesting is how the electronic, magnetic, and chemical properties of nanographene, which depend on the edge geometry, vary in the graphenization process. Prior to fusion, the edges, which are terminated by oxygen-containing functional groups, which, due to being handled in the ambient atmosphere, need to be stripped in the graphenization. Accordingly, fixing both geometry and chemical details at the edges is crucial to understand this graphenization process.

In connection to the edge chemistry, previous works on thermogravimetric (TG) and temperature programmed desorption (TPD) analyses[12,13] suggest that the following scenario in the change of the functional groups in ACFs depending upon heat treatment temperature (HTT): The pristine ACFs sample handled in the ambient atmosphere has oxygen-containing functional groups bonded to the edge carbon atoms and molecules, such as H_2O, physisorbed into nanopores. In the low HTT range, the desorption of adsorbed molecules and the decomposition of the carboxyl group (–COOH), weakly bonded to the edges, takes place up to 400 K and 600 K, respectively. In the HTT range from 600 K to 1100 K, the majority of functional groups become the carbonyl (>C=O) and phenol (–OH) groups, which are strongly bonded. Above 1500 K, heat treatment leads to fusion of the nanographene sheets after all the functional groups have been removed from the edges.

In the meantime, previous studies have reported interesting variations in the electronic and magnetic properties upon heat treatment.[14,15] In ACFs, the electron hopping between nanographene sheets governs the electron transport with the behavior of a Coulomb-gap-type variable range hopping in an Anderson insulator. The randomness in the network, with the barriers at the edges decorated with functional groups, then brings about the electron localization. Heat treatment up to 1500 K induces the decomposition of functional groups bonded to the edge carbon atoms, so that it enhances the electrical conductance because of the reduction of the hopping barriers. Higher HTT leads to an insulator-to-metal (IM) transition in the electron transport around the IM transition temperature T_{IM} = 1500−1600 K,[2] at which fusion makes the coherent electron transport network infinite, as indicated by the increase in the nanographene sheet size. This heat-treatment induced change in the electron transport is also reflected in the magnetic behavior. The edge-state spins of nanographene behave as localized spins interacting with each other through strong intra-nanographene-sheet and weak inter-nanographene-sheet exchange interactions, observed as effective Curie-Weiss behavior up to T_{IM}. In contrast, above T_{IM}, the edge state spins

disappear and instead the orbital susceptibility governs the magnetism.

Previous papers on the heat treatment process mentioned above can explain comprehensively the relationship between edge chemistry, electron transport, and magnetism.[12–15] However, there is a drawback in the experiments and also an important issue remaining to be clarified, regarding the interplay between electron transport, electronic structure, and edge-state-spin magnetism. The present scenario is based on experiments carried out independently, and in addition, there is a lack of information on the edge chemistry in the temperature region above 1100 K. Moreover, the relationship between the edge states and the edge-state spins remains to be clarified, in the latter of which the exchange interaction is expected to govern the behavior significantly. It is particularly important to carry out *in-situ* experiments of the chemical analysis and physical properties under the same condition and without exposure to air to avoid the effect of ambient atmosphere. In addition, we should track the behavior of the edge state together with the electron transport measurement in order to know the role of the edge state. In the present study, we have combined the structural characterizations of TPD, X-ray photon spectroscopy (XPS), and NEXAFS with *in-situ* conductance measurements of ACFs in a wide HTT range up to 1800 K, by considering the previous study related to this study[14–18]. This will help us gain insights into what really happens at the nanographene edges in the heat treatment process toward fusion.

2. Experimental

We used commercially available ACFs (specific surface areas of 2000 m^2/g, FR-20, Kuraray Chemical Co.) prepared by activation of phenol-based precursor materials.

The TPD measurements were performed by a home-built system equipped with a quadrupole mass spectrometer (QMS, Transpector 2 H100m, INFICON). A bundle-of-fibers sample of ACFs was mounted on a sample holder, which was degassed at 1550 K for 1 hour at a pressure below 5×10^{-5} Pa, and cooled down to room temperature before experiments began. The vacuum chamber storing the sample holder was carefully pre-baked for 1 hour at 550 K after the pre-evacuation down to 1×10^{-4} Pa to maintain the sample temperature below 400 K. After a stabilization time of 1 hour for the pressure and temperature of the chamber, and after a pressure below 2×10^{-5} Pa was achieved, the sample temperature was raised to 2100 K at a heating rate of 10 K per a minute while recording the QMS signal.

The electrical conductance was measured by using a 2-probe method in the vacuum chamber under a pressure below 1×10^{-4} Pa, where a bundle of fiber sample of ACFs was mounted on a sample holder. The sample was heat-treated by self-heating in the electric current flowing for 15 minutes in a vacuum chamber at various HTTs, which was controlled in the range from 400 to 1800 K. The time evolution of the conductance was also measured during the processes of pre-degassing and cooling after the heat-treatment.

The XPS and NEXAFS measurements were performed in the measurement chamber maintained in ultrahigh vacuum (UHV: $\sim 10^{-7}$ Pa), which was connected to the electrical conductance measurement chamber via a gate valve. The fiber sample was mounted on a sample holder and heated by electric current for 15 minutes in UHV at various HTTs in the range from 400 K to 1800 K. The XPS spectra were measured at room temperature using non-monochromatized Mg K_α radiation (1253.6 eV) for the excitation and a hemispherical analyzer (Scienta R3000). The binding energy was calibrated using Au_{4f} = 84.0 eV from the foil sample. The carbon (C) and oxygen (O) K-edge NEXAFS spectra were measured at the soft X-ray beam line BL-7A in the Photon Factory in the Institute of Materials Structure Science. The NEXAFS spectra were obtained by measuring the sample photocurrent (total electron yield method) at room temperature. The photon energy was calibrated with respect to the C 1*s* to π* peak position of highly oriented pyrolytic graphite (HOPG) at 285.5 eV. The NEXAFS spectra were taken at normal X-ray incidence. The temperature of the sample was monitored by using a pyrometer in the conductance, XPS, and NEXAFS measurements.

3. Results

Figure 1 shows the results of the TPD measurements up to 2100 K. The desorption of H_2O, CO_2, CO, and H_2 is observed in the ranges of 400−1200 K [600 K], 400−1000 K [600 K], 400−1500 K [1200 K] and 1100−2000 K [1400 K] ([ ]: peak position), respectively. Since the sample was evacuated below 400 K prior to the TPD measurement, the physisorbed molecules, including water and hydrocarbons, had desorbed from the

ACFs. Thus, all the detected molecules came from the decomposition of functional groups chemically bonded to the nanographene edges in the ACFs. The present results of the TPD measurements agrees with the previously reported one,[12] in which the maximum measurement temperature was 1000 K. Consequently the previous report revealed only a part of the CO desorption, and more importantly, it did not refer to the H_2 desorption. The present TPD measurements up to 2100 K enable us to reveal clearly the entire desorption process of CO and H_2, providing comprehensive information on what chemical species terminate the edge carbon atoms according to the temperature, as no desorption was observed above 2000 K.

The steep growth of the CO_2 and the H_2O peaks around 600 K was associated with the decomposition of −COOH. As the CO_2 and the H_2O signals decreased, the CO peak started growing with a peak temperature around 1200 K. This growth of the CO peak was associated with the decomposition of >C=O, −OH, and C-O-C (epoxy) together with the beginning of the steep increase of the H_2 signal at 1100 K. Note that only the H_2 peak persists above 1500 K. This fact suggests that edge carbon atoms are primarily terminated by hydrogen atoms in this temperature range. The absence of any peak above 2000 K is suggestive of edges being stripped with dangling bonds. The peak of the TPD spectra was broad and asymmetric. In the case of nanoporous ACFs, the peak shape of the TPD spectra depends on the stability of the functional groups attached to the edge carbon atoms and diffusion of desorbed gas molecules in the nanopores. We assign the CO_2, H_2O, and CO peaks to the decomposition of −COOH, >C=O, –OH, and C−O−C but, there should be other minor contributions such as lactone, quinone, and strongly bound intercalated water[21]. In addition, diffusion of desorbed gas molecule is complex for ACFs. These facts lead to the broad peaks of the TPD spectra.

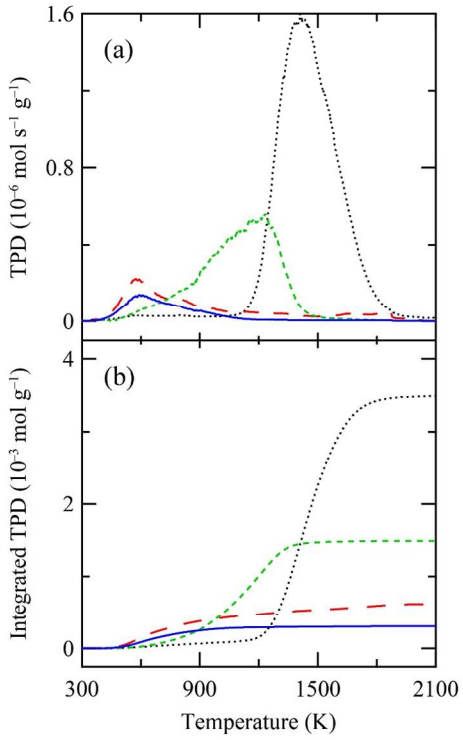

Fig. 1. (a) The TPD spectra and (b) integrated TPD intensities for the mass numbers of 2 (black dotted curve), 18 (red long-dashed curve), 28 (green short-dashed curve), and 44 (blue solid curve), corresponding to H_2, H_2O, CO, and CO_2, respectively.

Figure 1(b) shows the integrated intensities of the TPD signals for H_2O, CO_2, CO, and H_2 as a function of temperature. The proportions of the amount of H_2O, CO_2, CO, and H_2 were estimated to be 6:3:15:35 from the intensities. The amount of H_2 was much larger than that of other desorbed molecules. This excess of H_2 means that hydrogen is the major element constituting the functional groups, particularly at temperatures above 1500 K, as can be seen from the estimated H:O ratio 82 (=35×2+6×2) : 27 (=6+3×2+15). This high H:O ratio cannot be explained by considering only oxygen-containing groups. Even in the phenol group, the H:O ratio is 1:1. Accordingly, the present results prove that a large percentage of the edge carbon atoms were terminated with hydrogen even at low temperatures and that the hydrogen termination survived as the majority after most of the functional groups were decomposed above 1500 K.

One round piece of ~7 nm^2 (~3 nm in diameter) nanographene sheet is constituted by ~ 350 carbon atoms, in which about 1/4, namely ~90 atoms are distributed on the periphery. When we assume that the edge carbons are completely covered with hydrogens, the H/C mole ratio is 0.16, although the ratio slightly depends on the type of edge (zigzag or arm chair). Under this assumption, the amount of desorbed hydrogen molecules from 1 g of the ACFs is $1/2\times0.16\times1/12=6.7\times10^{-3}$ mol. As shown in Fig. 1b, the actual amount was 3×10^{-3} mol, which agreed with the expected value. This agreement supports the domain size of ACFs (~3 nm in diameter) and the number of the edge sites of the ACFs.

The conductance of the ACFs heated at various HTTs was measured at room temperature as a function of time during the cooling process after the heat treatment. This confirms the our previous results, which indicated the presence of an IM transition at T_{IM} = 1500−1600 K.[14,15] Figure 2 shows the resistance R_{HTT}/R_0 (R_0: the resistance of the

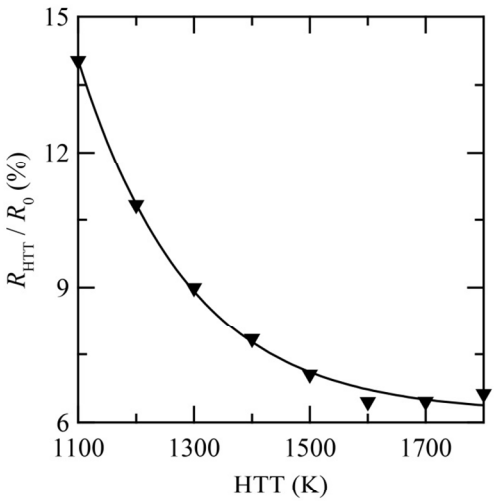

Fig. 2. The resistance of ACFs at room temperature as a function of HTT. The resistance (R_{HTT}) is normalized with respect to the resistance of the pristine sample (R_0). The solid curve is provided as a guide for the eyes.

pristine sample) of the ACFs at room temperature as a function of HTT from 1100 K to 1800 K, which covers T_{IM} and almost the entire desorption process of H_2. R_{HTT}/R_0 decreased steeply as HTT was elevated. It was approximately 14% for HTT = 1100 K, and it became roughly 6% in the region of the IM transition.

The characterization of the heat treated ACFs were performed using XPS. Figure 3(a) shows the C1*s* XPS spectra for the pristine ACFs and the ACFs heated at 1800 K. The C1*s* peak was observed at 284.4 eV, which was assigned to graphitic carbon,[22] with no fine structure. The C1*s* XPS spectra did not change with HTT. In the literature, the C1*s* peak has other components located at 286.5 eV, 287.5 eV, and 290.0 eV, which are assigned to the C−OH or C−O−C, >C=O, and −COOH functional groups, respectively.[23] Because the C1*s* XPS spectra did not have these peaks for the pristine sample nor changed upon heat treatments in the present measurements, the amount of such oxygen-containing functional groups was very small, even for the pristine sample. Figure 3(b) shows the O1*s* XPS spectra for the ACFs heated at various HTTs. The intensity of the O1*s* peak was large for the pristine ACFs, which was explained by weakly adsorbed molecules (e.g. water). The intensity of the O1*s* peak decreases sensitively with HTT, and becomes negligible above 1400 K. This HTT was close to the temperature above which the CO signal disappeared in the TPD spectrum (Fig. 1). The inset of Fig. 3(b) shows the peak deconvolution of the O1*s* XPS spectrum for the ACFs heated at 900 K. Double Gaussian curves were employed for the deconvolution with two peaks located at 531.0 eV and 533.5 eV corresponding to >C=O and C−OH or C−O−C, respectively. Accordingly, the oxygen-containing functional groups bonded to edge carbon atoms were assigned to >C=O, −OH, and C−O−C for the ACFs heated at 900 K, in good agreement with the previously proposed model based on the TPD measurements.[7,12] Furthermore, the disappearance of these two peaks above 1400 K confirmed the

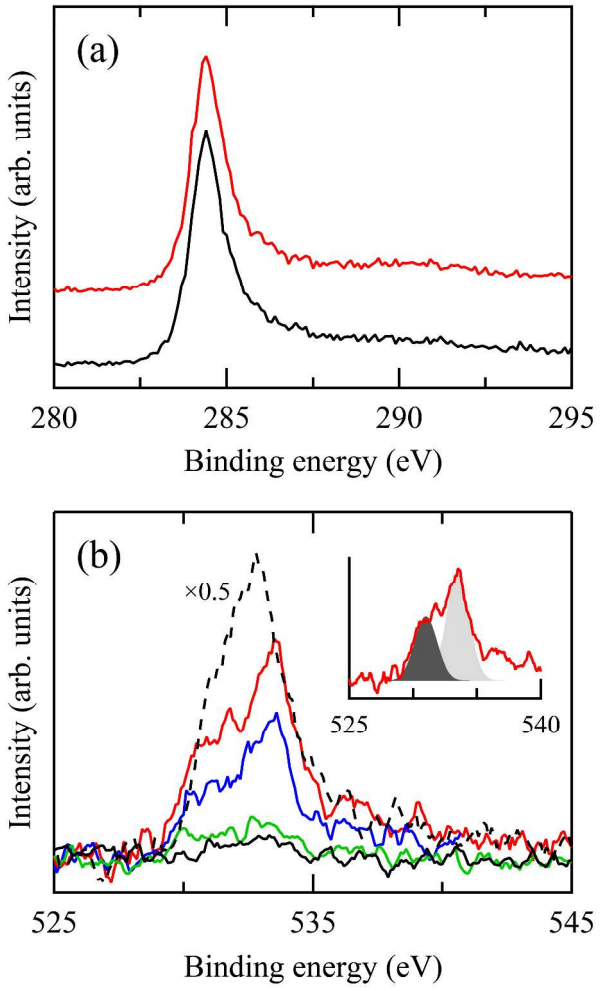

FIG. 3. (a) The C1*s* XPS spectra of the pristine ACFs and the ACFs heated at 1800 K denoted by black and red curves, respectively. (b) The O1*s* XPS spectra of the ACFs after heating at 900 K, 1100 K, 1400 K, and 1800 K, denoted by red, blue, green, and black curves, respectively. The dotted line is the NEXAFS spectra for the pristine ACFs. The inset shows double Gaussian fits to the spectrum of the ACFs heated at 900 K. The light-gray and the dark-gray ingredients originates from C−OH and >C=O, respectively.

absence of the oxygen-containing functional groups and that the majority of the edge carbon atoms were covered with hydrogen instead.

Figure 4 shows the O K-edge NEXAFS spectra of the ACFs after heat treatments at various HTTs. The normalization have not been performed. The edge jump, which is defined as the difference in the intensity of signal before and after the O K-edge, is proportional to the amount of oxygen atoms in the target sample.[22] Here again, the intensity of the peaks and the edge jump for the O K-edge NEXAFS spectra were large for the pristine ACFs. The edge jump decreases with HTT, indicating a decrease in the amount of oxygen contained in the ACFs. Figure 4(b) shows a close-up of the pre-edge region of the O K-edge NEXAFS spectrum of the sample treated at 900 K with the fitting results. The deconvolution comprised one step function (538.0 eV) and three Gaussian peaks located at 528.4 eV, 535.4 eV, and 539.7 eV, corresponding to the transitions from the O 1*s* to the $\pi^*_{C=O}$, $\sigma^*_{C-O,O-H}$, and $\sigma^*_{C=O}$ states, respectively.[23,24] The fit again shows that the oxygen-containing functional groups on edge carbon atoms of nanographene were >C=O and −OH and C−O−C for the ACFs heated at 900 K. It was difficult to perform the deconvolution of the O K-edge spectra for the ACFs heated above 1000 K owing to the insufficient amount of oxygen contained in the ACFs.

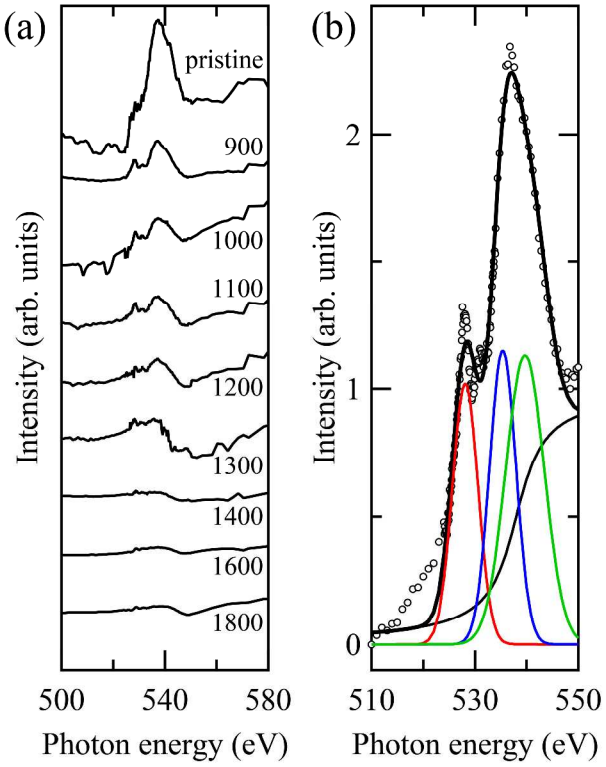

FIG. 4. (a) The O K-edge NEXAFS spectra of the ACFs after heat treatments at various HTTs. The spectra are parallel shifted along the vertical axis for clarity. (b) The close-up of the pre-edge region of the O K-edge NEXAFS spectrum of the ACFs heated at 900 K and the result of Gaussian fits, denoted as the circles and thick black curve, respectively. The deconvolution comprises three Gaussian peaks corresponding to $\pi^*_{C=O}$ (red curve), $\sigma^*_{C-O,O-H}$ (blue curve), and $\sigma^*_{C=O}$ (green curve) with a step function (thin black curve).

Figure 5(a) shows the C K-edge NEXAFS spectra of the ACFs after heat treatments at various HTTs. The NEXAFS spectra were normalized with respect to the value of the edge jump at 340 eV. All the spectra show two peaks, at 285.5 eV and 291.9 eV, corresponding to the transitions from the C 1*s* to the π* and σ* states, respectively.[22] Although it was reported that the contributions of relevant functional groups (i.e., >C=O, C−O, and C−H) typically appeared in the region of 287−291 eV by virtue of the transitions to the $\pi^*_{C=O}$, σ^*_{C-O}, and

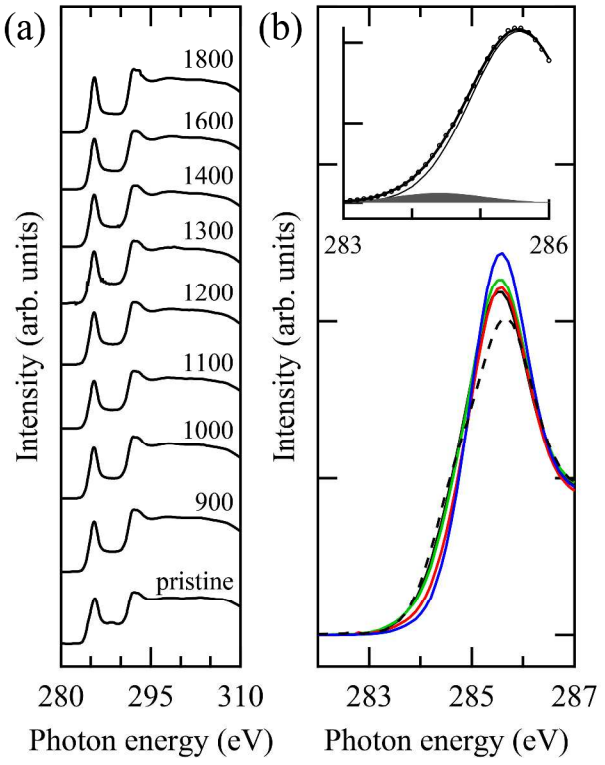

Fig. 5. (a) The C K-edge NEXAFS spectra of the ACFs after heat treatments at various HTTs. (b) The close-up of the pre-edge region of the C K-edge NEXAFS spectra of the ACFs heated at 900 K (black curve), 1400 K (green curve), 1600 K (red curve), and 1800 K (blue curve). The dotted line is the NEXAFS spectra for the pristine ACFs. The inset shows the spectrum of the sample heated at 900 K (circles) and double Gaussian fits (thin line and dark-gray region). The sum of the two Gaussian peaks is denoted by the solid curve.

σ^*_{C-H} states,[25−29] these transitions are not observed in the present measurement as shown in Fig. 5(a). In addition, the spectral features hardly changes in spite of the heat treatments. Thus, we have confirmed the small ratio of the carbon atoms bonded to >C=O, –OH, and C−O−C to the graphitic carbons in the ACFs samples in accordance with the C1*s* XPS spectra shown in Fig. 3(a). However,

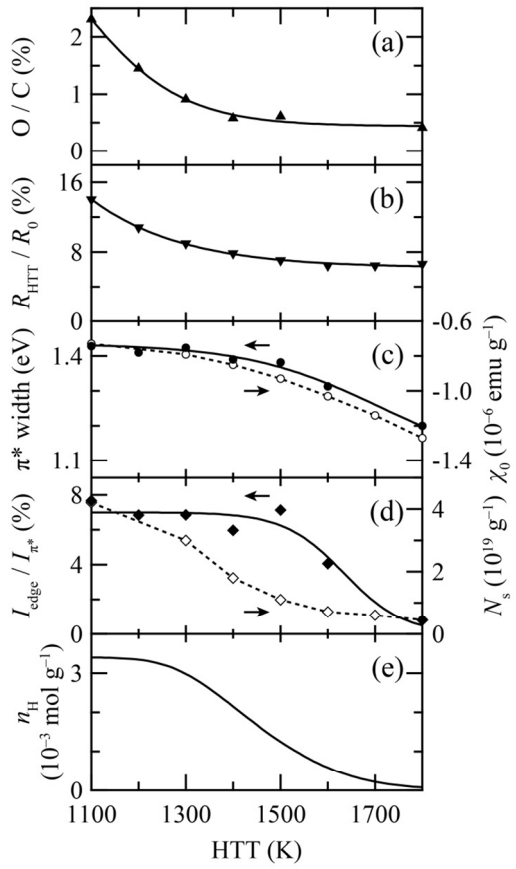

Fig. 6. The variation of (a) the intensity of the XPS O1*s* peak normalized with the C1s peak, (b) the resistance of the ACFs normalized with the value of the pristine sample, (c) the width of the π* peak, (d) the integrated intensity of the edge state peak normalized to the NEXAFS π* peak, and (e) the content of hydrogen bonded to the nanographene edges, as a function of HTT. The black symbols denote the data obtained experimentally and the solid curves are guides for the eyes, except for the solid curve in (e), which denotes the experimental data. The previously reported magnetic measurements [(c): orbital diamagnetic susceptibility: χ_0, (d) spin density: N_s] are also

taking a careful look at the pre-edge region of the C K-edge NEXAFS spectra, we find a reduction of the width of the π* peak with HTT, together with an increase in the intensity of the π* peak as shown in Fig. 5(b). The inset of Fig. 5(b) shows the C K-edge NEXAFS spectrum of the sample treated at 900 K and the curve fitting result, assuming that the energy of the π* peak was same as that of HOPG, similar to our previous works.[8,9] The deconvolution comprises two Gaussian peaks at 284.5 eV and 285.5 eV, which correspond to the edge state and the π* state, respectively.[8,9] The integrated intensity of the edge state peak is 7% of that of the π* peak for the pristine ACFs, which agrees with the

previously reported result within error bars.[9] Based on this result, we can roughly estimate the edge structure of the ACFs. Because only zigzag edges lead to the edge state peak in NEXAFS spectra, about 30 % of the edges were zigzag and 70 % of the edges were armchair. The introduction of dopants to graphene could also lead to the appearance of the additional pre-edge peak in the NEXAFS spectra[30]. However, the pre-edge peak was observed even for the ACFs heated above 1500 K, where there was little charge transfer between molecules and nanographene, which supported that the pre-edge peak originated from the edge state.

4. Discussion

Previous research gave us an idea about how the electronic and magnetic structures of networked graphene sheets are changed in the heat treatment process. Specifically, decomposition of various functional groups bonded to the edge carbon atoms and ensuing fusion of graphene sheets take place according to the heat treatment temperature.[12−15] Indeed it was revealed that an IM transition at T_{IM} = 1500−1600 K was triggered by the fusion process. Importantly, it is accompanied by the edge-state spins forming a spin glass state. Above that temperature region, the orbital susceptibility is enhanced at the expense of the edge state, the former and the latter of which are the signatures of the extension of π-conjugation and zigzag edges, respectively. This demonstrates that the fusion plays an important role in the changes of the electronic and magnetic properties. However, in this scenario it is not possible to get information about the relationship between the chemical structure and the electronic structure, particularly in the HTT region, where the IM transition takes place together with the fusion of the nanographene sheets. The present work uses NEXAFS as the important tool for the electronic structure investigation and the TPD and XPS investigations to cover the region in which the fusion takes place. This provides the necessary important information on the chemical structure-electronic structure relationship, in addition to the collective magnetic behavior of the edge-state spin system. Thus, our understanding of the scenario can now be more comprehensive and defect-free.

Let us summarize the experimental results of the present and previous investigations to get information on the relationship between the chemical and electronic structures. Figure 6 shows the results of the *in-situ* conductance and electron spectroscopic measurements and the TPD spectrum in the HTT region of 1100−1800 K. It shows the intensity of the O1*s* peak normalized to the C1*s* peak (O/C) in the XPS spectra, resistance of the ACFs normalized with the value of the pristine sample (R_{HTT}/R_0), the width of the π* peak and integrated intensity of the edge state peak normalized to that of the π* peak (I_{edge}/I_{π^*}) in the C K-edge NEXAFS spectra, and the amount of hydrogen bonded to nanographene edges (n_H). In addition, it also incorporates the previously reported results for the orbital susceptibility (χ_0) and the effective concentration of edge-state spins (N_s).[12] Note that the magnetic properties investigation in the previous work[14] was carried out without exposure to air during the entire measurement, as in the present work. Accordingly, the magnetic data in the previous work can be utilized together with the present results. As explained in the previous section, in the pristine ACFs, the peripheries of the nanographene sheets were covered predominantly with hydrogen atoms together with −COOH, >C=O, –OH, and C−O−C. Heat treatment led to the decomposition of –COOH, weakly bonded to the edge carbon atoms at around 600 K, and then the decomposition of >C=O, –OH, and C−O−C which was nearly completed at 1500 K as revealed by the TPD measurement (Fig. 1). Note that O/C reached the limit of detection at around 1300 K as shown in Fig. 6(a). Thus, we conclude that >C=O, –OH, and C−O−C were almost completely removed in the HTT range from 1300 K to 1500 K. Moreover, the removal of >C=O, −OH and C−O−C was tracked with fidelity by the reduction in the electrical resistance shown in Fig. 6(b). Indeed, the complete disappearance of oxygen content around 1300 K led to a less HTT dependent resistance, which became 6−7% of that in the pristine sample at 1800 K. Thus, this coincidence of the extinction of the oxygen-containing groups and the remarkable reduction in the resistance indicates that the negatively charged bulky oxygen-containing functional groups play an important role as a barrier for electron hopping between nanographene sheets.

An important issue to be discussed is at what temperature the fusion actually starts in the heat treatment process. We can discuss this issue in terms of the changes in the π* peak width and I_{edge}/I_{π^*} in the NEXAFS spectra, and n_H calculated from the TPD results, together with the previously reported values of χ_0 and N_s. Figures 6(c) and 6(d) show the evolution in the π* width and I_{edge}/I_{π^*},

respectively. Both of them obviously start decreasing at 1500 K.

The peak width in the NEXAFS spectra depends on the energy resolution of the beam line (0.3eV in the present setup), uniformity of the electronic structure of the atoms which is excited by photon, life time of the core hole, and other effects.[22] Along with the increase in the size of nanographene, the number of the interior carbon atoms increases, which leads to the increase in the uniformity of the electronic structure of carbon atoms. Thus, π* width decreases with HTT, reflecting the extension of the nanographene sheets. The peak intensity in NEXAFS spectra is roughly proportional to the density of states of certain electronic state (i.e. π state or edge state).[22] I_{edge} and I_{π^*} are proportional to the numbers of the interior carbon atoms and zigzag edge carbon atoms, respectively. As a consequence, the reduction in I_{edge}/I_{π^*} means the decrease in the edge carbon atoms. Therefore, both changes in the π* width and I_{edge}/I_{π^*} indicate the fusion of nanographene sheets. These findings are in good agreement with the presence of the IM transition previously reported to be triggered by fusion.[14,15] Furthermore, the present TPD measurement has clearly revealed the importance of the H_2 desorption for the fusing process. Figure 6(e) shows that n_H starts decreasing above 1300 K and becomes negligible around 1800 K. Note that the reduction in n_H is attributed to the decomposition of −OH in the HTT region of 1300−1500 K, and the removal of hydrogen atoms from the edges above 1500 K. The behavior of the amount of hydrogen has a quantitative trend almost identical with the ones for the π* width and I_{edge}/I_{π^*}. This coincidence demonstrates that the removal of hydrogen from the edges starting around 1500 K immediately brings about the fusion in a concerted manner. The simple chemical structure of edges bonded with hydrogen atoms after the complete removal of oxygen-containing functional groups facilitates the fusion above 1500 K. Moreover, above 1800 K, at which no hydrogen remains bonded, the fusion gives sufficiently grown nanographene sheets, for which the contribution of the edge state is negligible. As shown in Figs. 6(c) and 6(d), the π* peak width and the orbital susceptibility, both of which represent extensions of the π-conjugation, have the same variation with I_{edge}/I_{π^*} depending on HTT, except that χ_0 has a slight decrease far before T_{IM}. Taking into account that the absolute value of χ_0 ($|\chi_0|$) decreases upon the charge transfer from/to dopants due to the Fermi level shift from the Dirac point,[31] the slight decrease in χ_0 (increase in $|\chi_0|$) can be understood in terms of the declination of charge transfer to the oxygen-containing functional groups upon the removal of the functional groups as evidenced in the O/C ratio (Fig. 6(a)). The behavior of the π* peak width and χ_0 above T_{IM} demonstrates that the π-conjugation becomes extended successively in the fusion process at the expense of the edges. This explanation of the fusion is in good agreement with the increase of the nanographene size observed in the G/D ratio in the Raman bands in previous work, although the Raman experiment was carried out in ambient atmosphere, not meeting the conditions of the present work.[12]

The IM transition is at stake in an in-depth discussion regarding the fusion. The fusion starting near T_{IM} is initiated by the formation of a local π/sp^2 bond between the edge carbon atoms of adjacent nanographene sheets. The nanographene sheets, which are then weakly interacting with each other against the barriers of functional groups, are being successively and randomly networked through the π/sp^2 bond bridges in the percolative manner.[32] The local π/sp^2 bond as a strong electronic interaction can work to extend the π-conjugation between the nanographene sheets concerned, though the edge states in the edge region still exist. As the temperature approaches T_{IM}, the number of nanographene sheets participating in the π/sp^2 bridge network grows, and finally the network becomes infinite at T_{IM}, at which the percolation limit is achieved. The infinite sized network of nanographene sheets contributes to the coherent electron transport in the metallic state above T_{IM}. Further heat treatment at higher HTT makes nanographene sheets merge with the successive disappearance of the edges possessing edge states.

Finally, we discuss the behavior of the edge-state spins in relation to the fusion process. Here it should be noted that the HTT dependence of N_s is different from that of I_{edge}. The former is estimated as the effective spin concentration from the Curie-Weiss plot at an applied magnetic field of H = 1 T. Indeed, N_s starts decreasing well before I_{edge} decreases. This discrepancy is somewhat inconsistent, since the magnetic moment of the edge state is expected to be independent of HTT. The difference between I_{edge} and N_s can be understood based on the development of an exchange interaction acting between the edge-state spins of adjacent nanographene sheets. Below T_{IM}, the

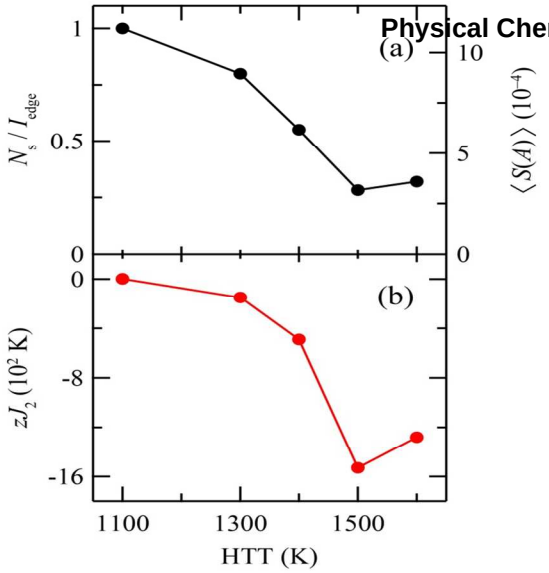

Fig. 7. (a) Effective edge-state spin concentration per edge state (N_s/I_{edge}) normalized to the ratio at HTT = 1100 K and the thermally average of edge-state spin <*S*> as a function of HTT. (b) Inter-nanographene-sheet interaction zJ_2 as a function of HTT.

nanographene sheets are independent from each other, although a weak electronic interaction, which is responsible for the electron hopping, exists. Consequently, the exchange interaction between edge-state spins in the individual nanographene sheet should be the main factor in the change in the observed magnetic moments. According to previous work,[33] the cooperation of the strong intra-zigzag-edge ferromagnetic interaction J_0 and the intermediate strength inter-zigzag-edge antiferromagnetic/ferromagnetic interaction J_1 results in a ferrimagnetic structure with nonzero net magnetic moment in the individual nanographene sheet, which behaves as a superparamagnetic nanoparticle. Upon the raising of HTT, the fusion of nanographene sheets starts near T_{IM}, where the formation of a local π/sp^2 bond at the edges between adjacent nanographene sheets develops. This gives a strong electronic interaction, which not only enhances the inter-nanographene electron transport, but also bridges between the edge-state spins on the adjacent nanographene sheets as an exchange interaction. It brings about a magnetic short range ordering toward a spin glass state as observed in previous studies.[14,15] Figure 7(a) gives the effective edge-state spin concentration per edge state as represented by N_s/I_{edge} normalized to the ratio at HTT = 1100 K as a function of HTT. We plot the data up to 1600 K, since both N_s and I_{edge} are small, and thus it is hard to obtain a reliable N_s/I_{edge} value. N_s/I_{edge} decreases steeply upon raising HTT. This is an important indication of the enhancement of an antiferromagnetic internal field acting between the edge-state spins of different nanographene sheets. The effective edge-state spin concentration N_s is being reduced steeper than the edge state concentration N_{edge}. The latter is proportional to I_{edge}. The internal field using the molecular field approximation can be estimated with the equation below, taking into account that the behavior of the ferrimagnetic moment of the individual nanographene sheet can be simplified. Thus, the spins of S = 1/2 interacting with weak inter-nanographene antiferromagnetic exchange interaction [$zJ_2 \sim -2$ to -3 K (*z*: number of neighboring nanographene sheet with respect to the nanographene sheet concerned)] for the ACFs up to 1100 K;[14]

$$\langle S(A) \rangle = \frac{M(A)}{N_{edge} g \mu_B} = S B_S \left(\frac{g \mu_B S (H + A \langle S(A) \rangle)}{k_B T} \right), \qquad (1)$$

where $\langle\ \rangle$ is the thermal average. In addition, S, M, N_{edge}, g, μ_B, and A in the Brillouin function $B_S(x)$ denote the edge-state spin, magnetization, edge state concentration, g-value (g~2), Bohr magneton, and internal exchange field, respectively. The last of these is proportional to the exchange interaction J_2 between the nanographene sheets;

$$A = \frac{2zJ_2}{g\mu_B}. \qquad (2)$$

In reality, the ferrimagnetic moment of the edge-state spins depends on the size and shape of the individual nanographene sheet. Consequently, we should take an ensemble average for the distribution of the ferrimagnetic moments in all of the constituent nanographene sheets having different sizes and shapes. However, the rather complicated procedure of the ensemble average is less informative and instead the simplification of a unique S can allow us to give the magnitude of the exchange interaction J_2.[26] Using the concentration of the edge states N_s at HTT = 1100 K, at which J_2 is negligible ($zJ_2 \sim -2$ to -3 K) and consequently $N_s(1100) = N_{edge}(1100) \propto I_{edge}(1100)$, the estimation of zJ_2 is given as a function of HTT as shown in Fig. 7(b), in which T = room temperature (300 K) and the applied field H = 1 T. In the estimation, $M(A=0)$ and $\langle S(A=0) \rangle$ are obtained from the above equation with HTT = 1100 K under the simplification that the internal field of the sample treated at HTT = 1100 K is negligible ($zJ_2 \sim -2$ to -3 K). The sign of zJ_2 is antiferromagnetic and its strength becomes increasingly steep as HTT approaches 1500−1600 K, where the strength is estimated as $zJ_2 \sim 1600$ K. Because of the strengthening of the exchange interaction between nanographene sheets, a short

range antiferromagnetic ordering develops in the nanographene sheets randomly networked through the exchange interaction, which is mediated by the local π/sp^2 bond bridge. Interestingly, the π/sp^2 bond bridge can create a strong antiferromagnetic exchange interaction ranging from 10^2 to 10^3 K between nanographene sheets. This is comparable with the intra-nanographene sheet interactions J_0 and J_1[26] and participates in the formation of a collective spin structure of the networked nanographene sheets. In the vicinity of the IM transition at the percolation threshold, the network becomes infinite, giving a spin glass state as observed.[14] Here the weak magnetic anisotropy of carbon having a negligible spin-orbit interaction of 5 cm^{-1} together with the serious randomness in the exchange interaction network causes the spin glass temperature to be lowered to ~7 K.[14] In the further development of the π/sp^2 bond bridge network upon fusion above the percolation threshold, the fusion works to merge the nanographenes sheets, bringing about the formation of a continuous graphene sheet with negligible edge contribution. The edge state spins disappears accordingly.

5. Conclusions

We have investigated the heat-treatment-induced variation of the electronic and magnetic structures in the network of nanographene sheets using electron transport, NEXAFS, XPS, and TPD measurements with the employment of ACFs and with the assistance of the magnetic data presented in previous work.

The edges of the nanographene sheets in the pristine ACFs are mainly bonded to hydrogen atoms together with the oxygen-containing functional groups of −COOH, >C=O, –OH, and C−O−C. Heat treatment first removes –COOH around 600 K and then >C=O, −OH, and C−O−C the removal of which is completed in the HTT range of 1300−1500 K. The removal of the oxygen-containing functional groups brings about a drastic increase in the conductance due to the lowering of the barriers in the electron hopping transport between nanographene sheets. Above 1500 K, the fusion of nanographene sheets starts occurring, which is confirmed by the reduction in the π* peak width and I_{edge}/I_{π^*} in the NEXAFS spectra upon the elevation of HTT, along with the previously reported increase in the absolute value of the orbital susceptibility. In addition, the present work has revealed that the removal of hydrogen atoms from the nanographene edges starts simultaneously with the fusion in a concerted manner. The edges bonded to hydrogen, which appears as the governing edge termination group above 1500 K after the disappearance of the oxygen-containing functional groups. This facilitates the fusion of nanographene sheets. In the percolative fusion process with the development of local π/sp^2 bond bridges between nanographene sheets, an IM transition takes place at the percolation threshold (HTT = 1500−1600 K), at which the continuous π/sp^2 bond network becomes infinite, accompanied with the development of a spin glass state of edge-state spins. The different heat-treatment-induced behaviors between the edge state peak intensity in NEXAFS and the effective concentration of the edge-state spins demonstrates a magnetic short range ordering as a precursor in the development of the spin glass state. Further heat treatment at higher HTT above 1800 K leads to the merge of nanographene sheets accompanied with the disappearance of the edge state.

Acknowledgements

The present work has been performed under the approval of the Photon Factory Program Advisory Committee PF-PAC, No. 2009G022. The authors are also grateful for the financial support of a Grant-in-Aid for Scientific Research, Grant No. 20001006 from the Ministry of Education, Culture, Sports, Science, and Technology of Japan. We thank Prof. Kenta Amemiya, KEK for assistance during the NEXAFS experiments.

Notes and references

[a] *Department of Chemistry, Graduate School of Science and Engineering, Tokyo Institute of Technology, Ookayama, Meguro-ku, Tokyo 152-8551 Japan.* mail: kiguti@chem.titech.ac.jp, tenoki@chem.titech.ac.jp

[b] *Institute of Multidisciplinary Research for Advanced Materials, Tohoku University, Aoba-ku, Sendai, Miyagi 980-8577, Japan.*

[†] *Present address: Department of Chemical Science and Technology, Faculty of Bioscience and Applied Chemistry, Hosei University, 3−7−2 Kajino-chou, Koganei, Tokyo 184−8584, Japan.*

Notes and References

1 K. S. Novoselov, A. K. Geim, S. V. Morozov, D. Jiang, Y. Zhang, S. V. Dubonos, I. V. Grigorieva, and A. A. Firsov, Science 2004, **306**, 666.
2 T. Enoki and T. Ando, *Physics and Chemistry of Graphene: Graphene to Nanographene* (Pan Stanford Publishing, Singapore, 2013).
3 P. Serp, M. Corrias, and P. Kalck, Appl. Cata A 2003, **253**, 337.
4 X. Wang, L. Zhi, N. Tsao, Ž. Tomović, J. Li, and K. Müllen, Angew. Chem. Int. Ed. 2008, **47**, 2990.
5 M. Fujita, K. Wakabayashi, K. Nakada, and K. Kusakabe, J. Phys. Soc. Jpn. 1996, **65**, 1920.
6 Y. Kobayashi, K. Fukui, T. Enoki, K. Kusakabe, and Y. Kaburagi, Phys. Rev. B 2005, **71**, 193406.
7 T. Enoki and K. Takai, Solid State Commun. 2009, **149**, 1144.

8 V. L. J. Joly *et al.*, Phys. Rev. B 2010, **81**, 245428.
9 M. Kiguchi, K. Takai, V. L. J. Joly, T. Enoki, R. Sumii, and K. Amemiya, Phys. Rev. B 2011, **84**, 045421.
10 M. S. Dresselhaus, A.W. P. Fung, A. M. Rao, S. L. di Vittorio, K. Kuriyama, G. Dresselhaus and M. Endo: Carbon 30 (1992).
11 K. Oshida, K. Kogiso, K. Matsubayashi, K. Takeuchi, S. Kobori, M. Endo, M. S. Dresselhaus, and G. Dresselhaus, J. Mater. Res., 10, 2507 (1995).
12 G. U. Sumanasekera, G. Chen, K. Takai, J. Joly, N. Kobayashi, T. Enoki, and P. C. Eklund, J. Phys. Condens. Mat. 2010, **22**, 334208.
13 N. Li, X. Ma, Q. Zha, K. Kim, Y. Chen, and C. Song, Carbon 2011, **49**, 5002.
14 Y. Shibayama, H. Sato, T. Enoki, and M. Endo, Phys. Rev. Lett. 2000, **84**, 1744.
15 Y. Shibayama, H. Sato, T. Enoki, X. X. Bi, M. S. Dresselhaus, and M. Endo, J. Phys. Soc. Jpn. 2000, **69**, 754.
16 A. Ganguly, S. Sharma, P. Papakonstantinow, and J. Hamilton, J. Phys. Chem. C 2011, **115**, 17009.
17 M. Acik, G. Lee, C. Mattevi, A. Pirkle, R. M. Wallace, M. Chhowalla, K. Cho, and Y. Chabal, J. Phys. Chem. C 2011, **115**, 19761.
18 T. Shimizu, J. Haruyama, D. C. Marcano, D. V. Kosinkin, J. M. Tour, K. Hirose, and K. Suenaga, Nat. Nanotechnol. 2011, **6**, 45.
19 V. Lee, R. V. Dennis, C. Jaye, X. Wang, D. A. Fischer, A. N. Cartwright, and S. Banerjee, J. Vac. Sci. Technol. B 2012, **30**, 061206.
20 B. J. Schultz, R. V. Dennis, J. P. Aldinger, C. Jaye, X. Wang, D. A. Fischer, A. N. Cartwright, and S. Banerjee, RSC Adv. 2014, **4**, 634.
21 M. Acik, C. Mattevi, C. Gong, G. Lee, K. Cho, M. Chhowalla, and Y. J. Chabal, ACS Nano 2010, **4**, 5861.
22 J. Stöhr, *NEXAFS Spectroscopy* (Springer, New York, 1991).
23 O. Akhavan, Carbon 2010, **48**, 509.
24 D. Rosenthal, M. Ruta, R. Schlögl, and L. K. Minsker, Carbon 2010, **48**, 1835.
25 S. Banerjee, T. H. Benny, M. Balasubramanian, D. A. Fischer, J. A. Misewich, and S. S. Wong, Chem. Commun. 2004, **7**, 772.
26 A. Kuznetsova, I. Popova, J. T. Yates Jr., M. J. Bronikowski, C. B. Huffman, J. Liu, R. E. Smalley, H. H. Hwu, and J. G. Chen, J. Am. Chem. Soc. 2001, **123**, 10699.
27 A. Hoffman, A. Heiman, H. P. Strunk, and S. H. Christiansen, J. Appl. Phys. 2002, **91**, 3336.
28 T. Y. Kim, C. S. Lee, Y. J. Lee, K. R. Lee, K. H. Chae, and K. H. Oh, J. Appl. Phys. 2007, **101**, 023504.
29 S. Ohmagari, T. Yoshitake, A. Nagano, S. A. Riyami, R. Ohtani, H. Setoyama, E. Kobayashi, and K. Nagayama, J. Nanomaterials 2009, **2009**, 876561.
30 B. J. Schultz, *et al.*, Nat. Commun. 2011, 2, 372.
31 Y. Ominato and M. Koshino, Solid State Commun. 2013, **175–176**, 51.
32 S. Kirkpatrick, Rev. Mod. Phys. 1973, **45**, 574.
33 V. L. J. Joly, K. Takahara, K. Takai, K. Sugihara, T. Enoki, M. Koshino, and H. Tanaka, Phys. Rev. B 2010, **81**, 115408.

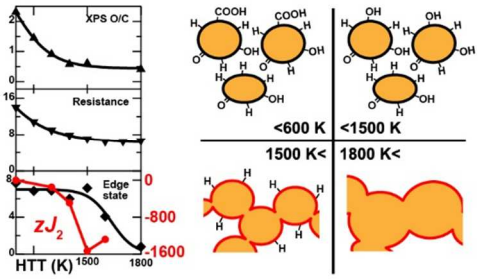

Verification of edge chemistry of nanographene sheets and development of antiferromagnetic interaction between the sheets upon heat treatment temperature (HTT).

TOC